The International Journal of Advanced Manufacturing Technology (2018) 95:3977–3984
https://doi.org/10.1007/s00170-017-1489-1

ORIGINAL ARTICLE

Thermal and molten pool model in selective laser melting process of Inconel 625

Erdem Kundakcıoğlu[1] · Ismail Lazoglu[1] · Özgür Poyraz[2] · Evren Yasa[3] · Nuri Cizicioğlu[2]

Received: 6 September 2017 / Accepted: 13 December 2017 / Published online: 3 January 2018

Abstract

Nowadays, additive manufacturing via topology optimization creates new opportunities for weight reductions in aerospace industry where high fly-to-buy ratio is desired. Selective laser sintering of advanced engineering materials like nickel super alloys are also expanding to reduce the cost and time of the manufacturing in aerospace industry. Elevated temperature and temperature gradients are critical factors in selective laser sintering of metals and they significantly affect the quality and integrity factors of produced parts such as microstructures, porosity, residual stresses, and distortions. Therefore, the aerospace industry needs advanced simulation tools to predict the temperatures, temperature gradients, and molten pool geometries to better understand the physics of the selective laser melting process as well as for the process optimizations. This article introduces an adjustable finite element-based multi-physics and multi-software platform thermal model, for laser additive manufacturing in powder bed systems to predict the transient temperature and the molten pool geometry. The developed model is able to simulate 3D transient temperature and molten pool shape in the laser additive manufacturing process by including the features of melting and solidification, porous media, and temperature-dependent thermal material properties for different materials. A set of experiments of Inconel 625 is carried out in order to measure the size of the molten pool and to validate the developed thermal model. An experimental study on temperature distribution carried out with titanium and an experimental study on molten pool sizes carried out with Inconel 625 in the literature are also compared with the developed thermal model. The estimation errors of the developed model are in the range of 11–18%.

Keywords Selective laser melting · Temperature distribution · Molten pool · Finite element analysis · Inconel 625, titanium

Nomenclature

ρ	Density
C_p	Heat capacity
k	Thermal conductivity
h	Heat convection coefficient
q	Input heat flux
$\hat{n}$	Unit normal vector
Q	Laser heat generation
P	Total laser power
η	Laser absorption coefficient
d	Diameter of the laser beam
x_0	Pulse center x-coordinate
y_0	Pulse center y-coordinate
z_0	Pulse center z-coordinate
h_p	Penetration depth of the laser
σ	Stefan-Boltzmann constant
k_{powder}	Thermal conductivity (powder)
k_{eq}	Effective thermal conductivity of powder bed
k_g	Thermal conductivity of gas (between particles)
k_s	Thermal conductivity of the skeletal solid
B	Deformation parameter of the particle ($B = 1$ when the particle surface is that of a sphere)
φ	Porosity
k_R	Conductivity by radiation
ϕ	Flattened surface fraction of particle in contact with another particle
$k_{contact}$	Contact conductivity between two particles according to the value of ϕ

✉ Ismail Lazoglu
ilazoglu@ku.edu.tr

[1] Manufacturing and Automation Research Center, Mechanical Engineering Department, Koc University, 34450 Istanbul, Turkey

[2] TUSAŞ Engine Industries Inc., 26003 Eskişehir, Turkey

[3] Eskişehir Osmangazi University, Department of Mechanical Engineering, 26003 Eskişehir, Turkey

T_{ext}	Gas medium temperature
T_{amb}	Room temperature
q_{rad}	Heat loss due to radiation
ε	Emissivity

1 Introduction

The metal additive manufacturing process, additive layer manufacturing (ALM), was introduced in the mid-1990s via the application of the high-energy density lasers [1]. This new technique allows manufacturing a part layer by layer by using 3D CAD information. As a result of this progress, manufacturing of 3D complex freeform geometries has become relatively easier, whereas with other conventional methods, this has been costly and time-consuming [2].

Although design flexibility is provided by additive manufacturing [3], an extensive research and development stage is required beforehand in order to achieve end-shape parts with the required mechanical properties. In metal additive manufacturing, high-temperature gradients appear on the manufactured structure due to the employment of high-energy density laser. These gradients affect the microstructure and physical properties of the part such as mechanical strength, surface, and overall quality of the parts.

The first step of controlling the mechanical properties of the additively manufactured parts is the prediction of the temperature distribution and molten pool geometry. Such a prediction tool is crucial from both industrial and scientific perspectives in order to optimize the manufacturing process.

The effects of the heat transfer mechanisms in the porous media undergoing phase changes are investigated in the literature by several mathematical and finite element techniques [4–16] in metal additive manufacturing. A mathematical model of a moving heat source on a medium was studied by Jeager [4]. In order to predict the final geometry, Huang et al. developed an analytical model for laser powder-fed systems [5]. Matsumoto et al. proposed a 2D finite element model to examine temperature development during single-layer process in powder beds for metallic powder [6]. Tolochko et al. investigated Nd: YAG laser sintering mechanism including powder melting [7]. Li et al. [8] did a parametric study of laser speed and laser power to investigate the thermal behavior during selective laser melting process. They carried out a series of experiments by using different laser powers and speeds in order to see the effects of these parameters on single-track scanning. A microstructure study was carried out by Farshidianfar et al. to control the microstructure in real time during laser additive manufacturing [9]. Kolossov et al. demonstrated the effect of the temperature-dependent thermal conductivity on the temperature gradients in a laser sintering using the 3D finite element model [10]. Another 3D transient finite element analysis was carried out by Nisar et al. to investigate phase change and moving heat source problem [11]. Roberts et al. carried out a study for powder beds to understand multilayer sintering mechanism with porosity and temperature-dependent material properties. The model specifically provided the remelted zones and temperature history for each layer [12]. Ganci et al. carried out a similar study for the selective laser sintering of thermoplastics to predict the temperature distribution and part distortion including phase transformations and cooling process [13]. Somashekara et al. investigated the effects of the deposition pattern on the residual stress evolution in metal additive manufacturing [14].

The purpose of this study is to introduce a FEM model for the powder bed system, from which the effects the material properties and scanning parameters on the temperature distribution and molten pool geometry during the metal additive manufacturing can be predicted. Including the powder—liquid—solid transformation and a 3D heat source model, the developed model can predict the temperature evolution and the dynamic molten pool geometry. In the literature, experiments carried out with titanium and Inconel 625 are available and the developed thermal model is compared with those experiments. A new set of experiments with Inconel 625 are conducted and their results are compared with those from the simulation. These are all found to be in good agreement within 11–18% error.

2 Thermal modeling

2.1 Heat equation

In the metal additive manufacturing process, a laser heats up and melts the powder material, forming a small molten pool (Fig. 1). After the laser moves from the molten zone, solidification starts and the generated heat dissipates by three ways: conduction, convection, and radiation. In the powder bed ALM system with moving laser source, the heat transport equation can be defined as

$$\rho C_p \frac{\partial T}{\partial t} = \nabla \cdot (k \nabla T) + q \tag{1}$$

Fundamental mode of Gaussian beam (TEM_{00}) is selected for the 3D heat source model in the Cartesian coordinate and it is written as

$$Q(x,y,z) = \frac{8\eta P}{\pi d^2} \exp\left(-\frac{8\left[(x-x_0)^2 + (y-y_0)^2\right]}{d^2}\right) \frac{1}{h_p} \exp\left(\frac{-abs(z-z0)}{h_p}\right) \tag{2}$$

The penetration depth of the laser h_p and the absorption coefficient η between the powder material and the wavelength of the laser, for Inconel 625 and Nd:YAG laser, are taken 110 μm and 0.37 [16], respectively, and for titanium and

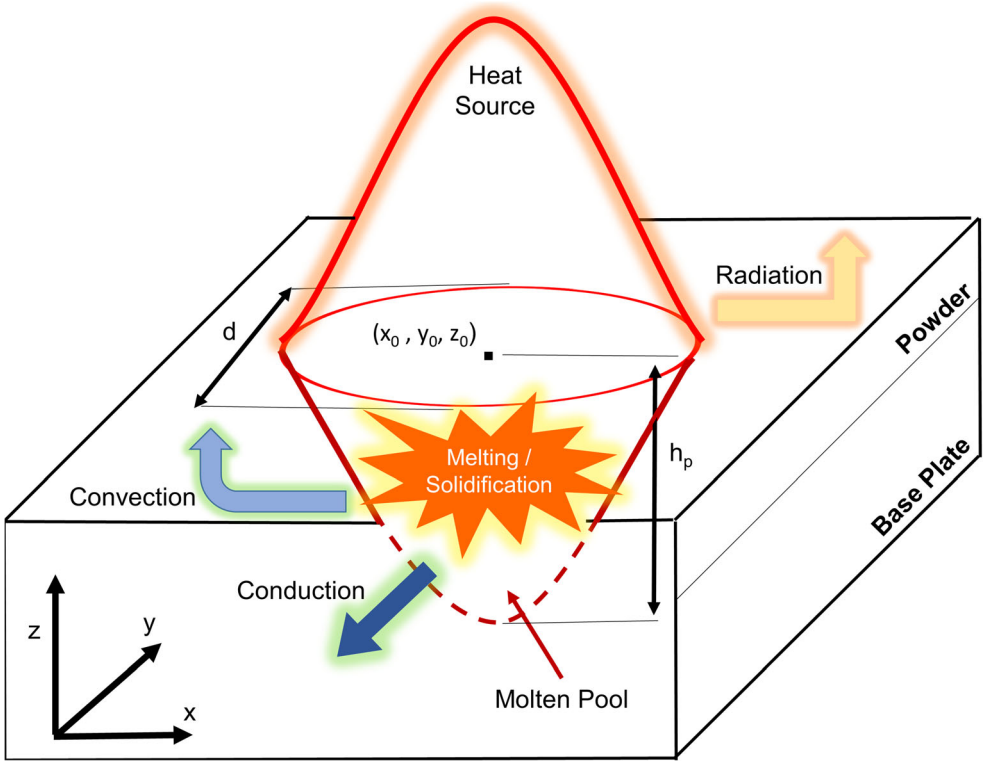

Fig. 1 Illustration of the heat zone in the powder bed ALM system

Nd:YAG laser, are taken 63 [10] μm and 0.42 [18], respectively.

Convection and radiation losses in the ALM process are expressed in Eqs. 3 and 4, respectively, as follows:

$$h(T_{ext}-T) = -\hat{n}\cdot -(k\nabla T) \tag{3}$$

$$q_{rad} = \varepsilon\sigma\left(T_{amb}^4 - T^4\right) \tag{4}$$

The phase transformation between solid and liquid phases of a material can be introduced into Eq. (1) with the following relations.

$$\rho = \theta\rho_{solid} + (1-\theta)\rho_{liquid} \tag{5}$$

$$C_p = \frac{1}{\rho}\left(\theta\rho_{solid}C_{p,solid} + (1-\theta)\rho_{liquid}C_{p,liquid}\right) + L\frac{da}{dT} \tag{6}$$

$$k = \theta k_{solid} + (1-\theta)k_{phase2} \tag{7}$$

$$a = \frac{(1-\theta)\rho_{liquid} - \theta\rho_{solid}}{\theta\rho_{solid} + (1-\theta)\rho_{liquid}} \tag{8}$$

where θ is the phase fraction (solid = 0, liquid = 1), L is the latent heat of phase change from solid to liquid and a is the mass fraction.

The Comsol Multiphysics heat module is used for the FEM implementation. In the module the heat Eq. (1) and the phase change Eqs. (5–8) are utilized as a platform for the integration of the heat source model and the powder bed material model. Furthermore, a script is written in order to simulate the melting and solidification during the additive manufacturing process (powder to liquid, solid to liquid and liquid to solid). The script introduces a phase transformation coefficient as a variable dependent on the temperature distribution. The role of this phase transformation coefficient is to hold the information of whether the powder is melted or not. In other words, the FEM model uses the temperature history and the melted zone history in order to decide which phase transformation will occur according to the temperature and the phase transformation coefficient in that zone.

The developed model can be adjusted for different types of materials and lasers using the phase transformation coefficient and laser penetration depth. A schematic of the developed model is given in Fig. 2.

2.2 Material properties

Thermal conductivity is significantly affected by porosity. Although, the thermal conductivity of bulk materials is dependent on temperature, the thermal conductivity of the powder bed is also dependent on powder geometry and the thermal conductivity of the protective gas. It is assumed that the powder is uniformly distributed; Sih et al. [17] proposed a detailed thermal conductivity model for powder beds, which includes the effects of porosity, emissivity, powder size, and protective gas conductivity. Equivalent thermal conductivity can be expressed as,

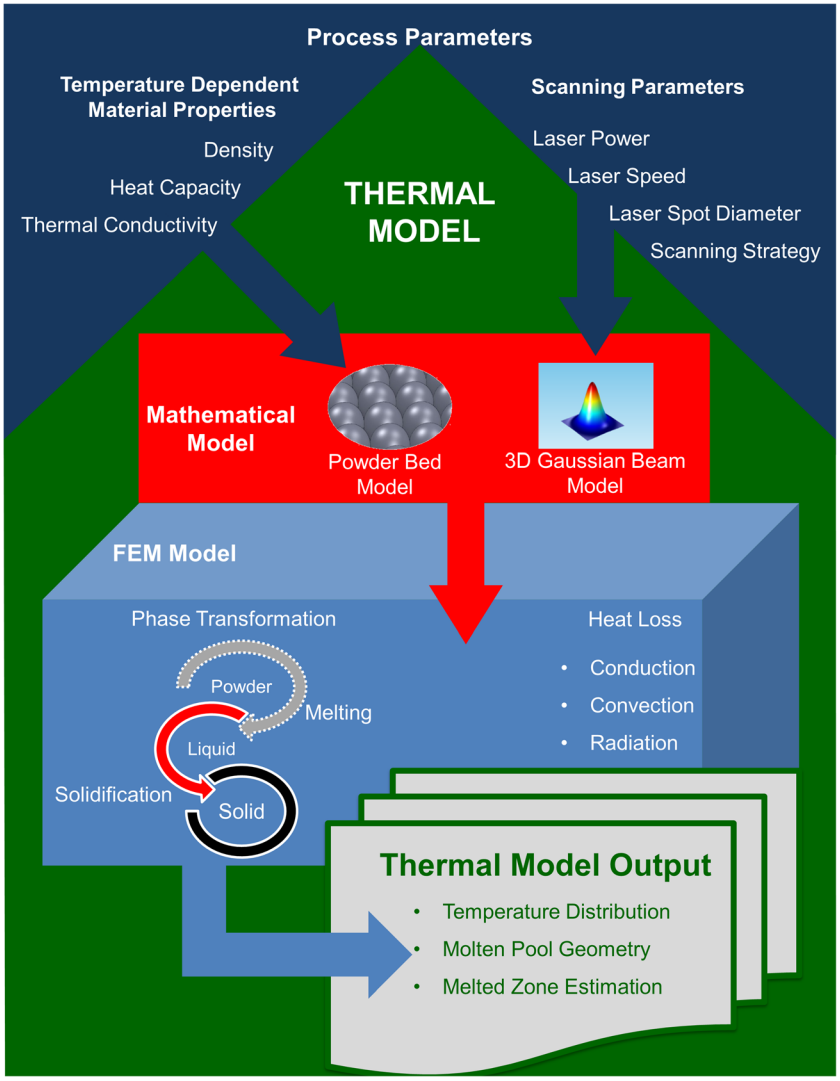

Fig. 2 Schematic of the multi-physics based thermal model

$$k_{eq} = k_g\left(1-\sqrt{1-\varphi}\right)\left(1+\frac{\varphi k_R}{k_g}\right) + k_g\sqrt{1-\varphi}\left\{(1-\phi)\left[\frac{2}{1-\frac{Bk_g}{k_s}}\left(\frac{B}{\left(1-\frac{Bk_g}{k_s}\right)^2}\left(1-\frac{k_g}{k_s}\right)ln\left(\frac{k_s}{Bk_g}\right)-\left(\frac{B+1}{2}\right)-\left(\frac{B-1}{1-\frac{Bk_g}{k_s}}\right)\right)+\frac{k_R}{k_g}\right]+\phi\frac{k_{contact}}{k_g}\right\} \quad (9)$$

The inclusion of temperature-dependent material properties in the model is one of the key points to predict the temperature in ALM process. Table 1 shows the temperature-dependent thermal conductivity and heat capacity of Inconel 625 used in the model.

Table 1 Material Properties of Inconel 625 [16]

Temperature, T (°C)	Thermal conductivity, k (W/m.K)	Heat capacity, C_p (J/kg)
20	9.9	410
93	10.8	427
205	12.5	456
315	14.1	481
425	15.7	511
540	17.5	536
650	19.0	565
760	20.8	590
870	22.8	620

3 Thermal model validation and discussion

The developed model is first compared to a work carried out by Kolossov et al. [10] on a 5 mm × 5 mm × 2 mm titanium powder block. The developed model can perform with

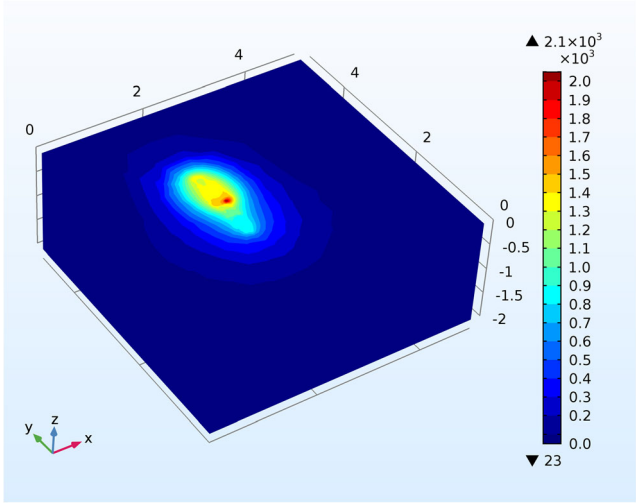

Fig. 3 The 3D temperature [°C] distribution of the 5 mm × 5 mm × 2 mm sample

different materials by using Eq. 9. The required material properties are taken from the literature [18]. With the process parameters of laser power, beam diameter, scanning speed, and powder size as 2 W, 0.025 mm, 1 mm/s, and 30 μm, the thermal model was simulated with the same conditions of the experiment. The 3D temperature distribution obtained from the developed model is shown in Fig. 3 and the comparison between the experimental and simulation results is shown in Fig. 4.

In order to validate the developed model, two experiments were conducted. Experiments were carried out on a direct metal laser sintering (DMLS) system which has a Fiber YAG laser with a wavelength of 1064 nm. Prismatic parts with the length of 50 mm, width of 10 mm, and height of 7 mm from EOS Nickel Alloy IN625 powder. The additively manufactured specimens were cut with wire electric discharge machining in order to obtain smaller pieces for metallurgical evaluation. The cut specimens were then mounted onto a bakelite puck, which had been polished with a grinder and chemically etched. Finally the microscopic investigation was conducted using NİKON/ECLIPSE MA200 optical microscope. Figure 5 shows the microscopic photos of the manufactured specimen which were taken using 200X magnification.

The thermal model was simulated with the same parameters and the simulation results are shown in Figs. 6 and 7. The width and depth of the molten pool are calculated, respectively, 155 and 129 μm.

Another experimental work on Inconel 625 was performed by Li et al. [8]. Four different types of laser track characteristic were obtained: discontinuous, semi-continuous, continuous, and smooth zone. To compare the experimental work and the developed model, the simulation is run with the scanning parameters for continuous zone characteristic (laser power and laser speed are taken as 65 W and 1500 mm/min, respectively). The experimental and simulation results of the laser track are shown in Fig. 8. The track width and penetration depth reported in the study are compared to the simulation results in Table 5.

The process parameters for the experiments and the studies found in the literature are listed in Table 2. The prediction errors for the experiments carried out in this study are listed in Table 3. The prediction errors for the studies found in the literature are listed in Tables 4 and 5.

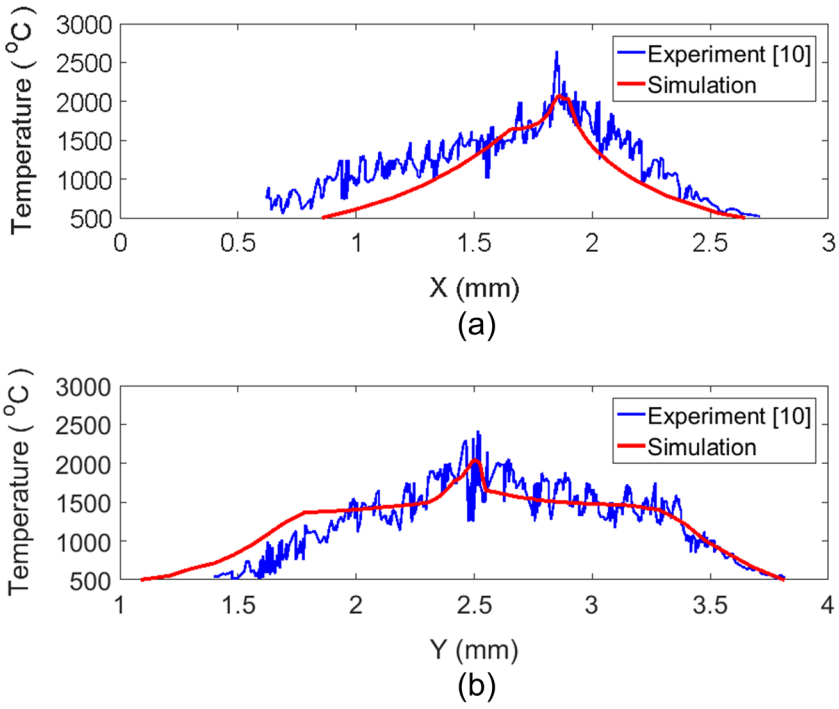

Fig. 4 The comparison between experimental and simulation results: (a) The temperature distribution of *x*-profile at $y = 2.5$ mm and $z = 2$ mm. (b) The temperature distribution of *y*-profile at $x = 1.85$ mm and $z = 2$ mm

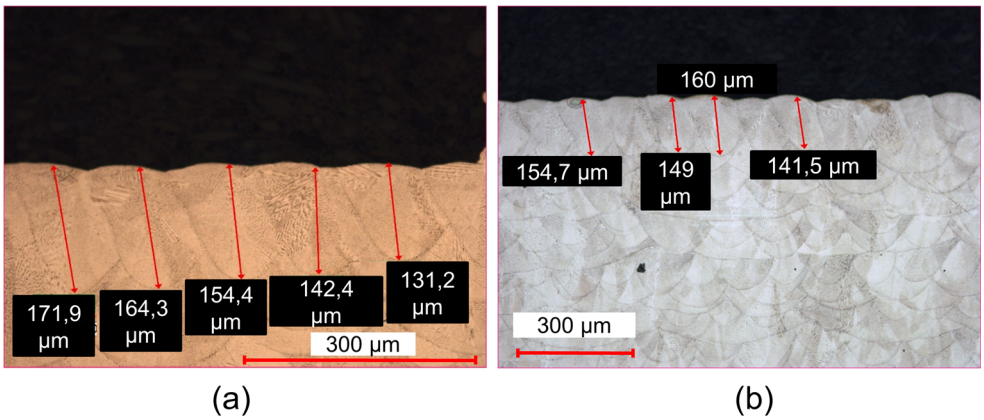

Fig. 5 Cross-sectional views of **a** first measurement and **b** second measurement

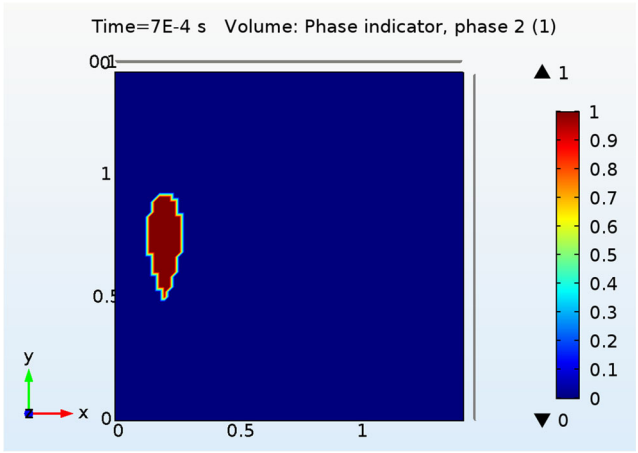

Fig. 6 Molten pool geometry in *x*- and *y*-directions

For the first comparison, the same scanning parameters and material reported in [10] are used in the developed model. The maximum temperature is predicted with 13.6% error. Moreover, as it can be observed from the Fig. 4, the temperature distributions in the *x*- and *y*-directions are agreeing well with each other. For the second comparison, the scanning parameters are shown in Table 2 and are used for the manufacture of the sample part. The sample part was cut with the wire electric discharge machining and the cut specimens were investigated with an optical microscope in order to measure the penetration depth. The results of the penetration depth of the developed model and the results of the experiments carried out in TEI are compared and the model satisfies the experimental results with 15% error. In addition, with the same material in use, the scanning parameters of the work of Li et al. [8] are tested in the developed thermal model. The track width prediction agrees with the reported results by 18% error and the penetration depth (reported as the sum of melted depth and track height) prediction agrees with the reported results by 11.7% error. As it can be seen from the experimental validations and the comparisons made from literature, the developed thermal model can predict the temperature and the molten pool region in the acceptable range.

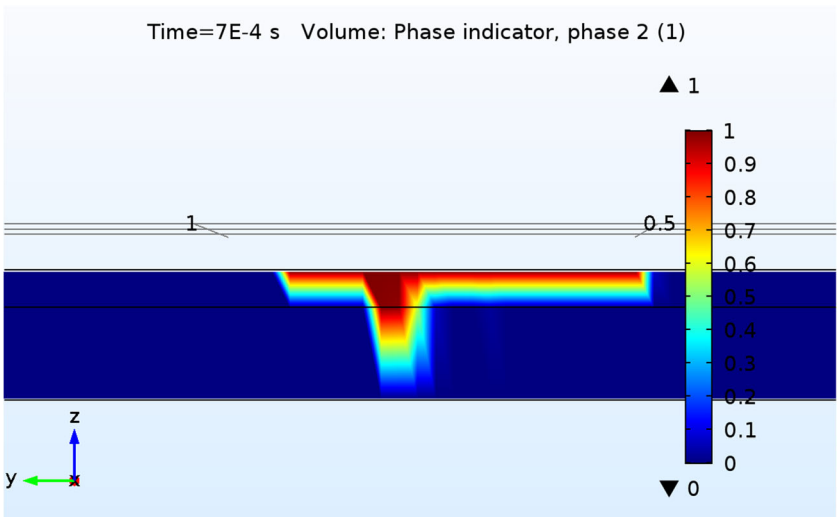

Fig. 7 Molten pool geometry in *y*- and *z*-directions

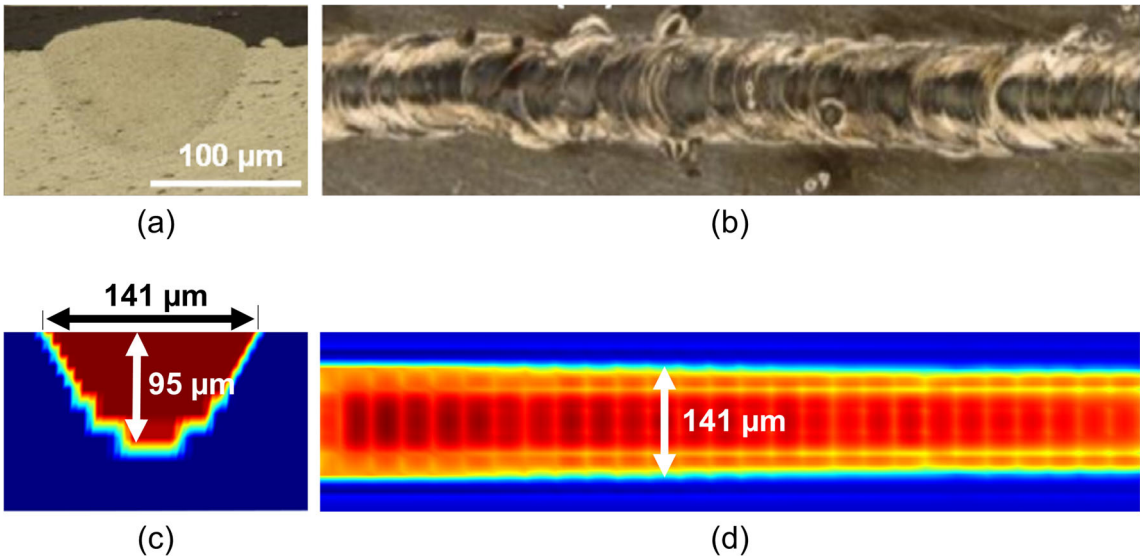

Fig. 8 Laser track results. **a** The cross-section (experimental). **b** The top view (experimental). **c** The cross-section (simulation). **d** The top view (simulation)

Table 2 Process parameters of the experiments and the studies found in literature

Process parameters	Laser power [W]	Laser speed [mm/s]	Laser spot size [μm]	Material
Experiment	200–300	900–1000	50–100	Inconel 625
Study from literature [10]	2	1	25	Titanium
Study from literature [8]	65	960	72	Inconel 625

Table 3 Comparison of the simulation and experimental results

	Penetration depth (μm)	Prediction error
Simulation	129	15.1%
Experimental	152.1	

Table 4 Comparison of the simulation and experimental results extracted from the literature [10]

	Maximum temperature (°C)	Prediction error
Simulation	2073	13.6%
Experimental	2400	

Table 5 Comparison of the simulation and experimental results extracted from the literature [8]

	Penetration depth/track width	Prediction error
Simulation	95 μm/141 μm	11.7%/18%
Experimental	85 μm/121 μm	

4 Conclusion

In this study, via 3D heat source modeling and phase transformation modeling, a 3D thermal model has been developed for the powder bed system. The developed model both contains analytical and FEM modeling in order to achieve appropriate predictions. The developed model is validated by a new set of experiments with Inconel 625 powder and also compared with the studies found in the literature. The prediction errors of the developed model are found to be in the acceptable range. The developed thermal model can be used to investigate the temperature distribution and the molten pool geometry for the additive manufacturing of 3D freeform complex geometries.

Acknowledgements The authors would like to thank the Undersecretariat for Defence Industries (SSM) of Turkey and Tusaş Engine Industries Inc. for supporting the project.

References

1. Levy GN, Ralf S, Kruth JP (2003) Rapid Manufacturing And Rapid Tooling With Layer Manufacturing (Lm) Technologies, State Of The Art And Future Perspectıves. CIRP Ann Manuf Technol 52(2):589–609. https://doi.org/10.1016/S0007-8506(07)60206-6
2. Bikas H, Stavropoulos P, Chryssolouris G (2016) Additive manufacturing methods and modeling approaches: a critical review. Int J Adv Manuf Technol 83:389–405. https://doi.org/10.1007/s00170-015-7576-2
3. Chen L, He Y, Yang Y, Niu S, Ren H (2017) The research status and development trend of additive manufacturing technology. Int J Adv Manuf Technol 89:3651–3660. https://doi.org/10.1007/s00170-016-9335-4
4. Jaeger JC (1942) Moving sources of heat and the temperature at sliding contacts. Proc R Soc 76:203–224

5. Huang Y, Khamesee MB, Toyserkani E (2016) A comprehensive analytical model for laser powder-fed additive manufacturing. Addit Manuf 12(A):90–99. https://doi.org/10.1016/j.addma.2016.07.001
6. Matsumoto M, Shiomi M, Osakada K, Abe F (2002) Finite Element Analysis of Single Layer Forming on Metallic Powder Bed in Rapid Prototyping by Selective Laser Processing. Int J Mach Tools Manuf 42(1):61–67. https://doi.org/10.1016/S0890-6955(01)00093-1
7. Tolochko NK, Arshinov MK, Gusarov AV, Titov VI, Laoui T, Froyen L (2003) Mechanism of Selective Laser Sintering and Heat Transfer in Ti Powder. Rapid Prototyp J 9(5):314–326. https://doi.org/10.1108/13552540310502211
8. Li C, Guo YB, Zhao JB (2017) Interfacial phenomena and characteristics between the deposited material and substrate in selective laser melting Inconel 625. J Mater Process Technol 243:269–281. https://doi.org/10.1016/j.jmatprotec.2016.12.033
9. Farshidianfar MH, Khajepour A, Gerlich AP (2016) Real-time control of microstructure in laser additive manufacturing. Int J Adv Manuf Technol 82:1173–1186. https://doi.org/10.1007/s00170-015-7423-5
10. Kolossov S, Boillat E, Glardon R, Fischer P, Locher M (2004) 3D FE simulation for temperature evolution in the selective laser sintering process. Int J Mach Tools Manuf 44(2–3):117–123. https://doi.org/10.1016/j.ijmachtools.2003.10.019
11. Nisar A, Schimidt MJJ, Sheikh MA, Li L (2003) Three-dimensional transient finite element analysis of the laser enamelling process and moving heat source and phase change considerations. Proc Inst Mech Eng B J Eng Manuf 217:753–764. https://doi.org/10.1243/09544050360673143
12. Roberts IA, Wang CJ, Esterlein R, Stanford M, Mynors DJ (2009) A three-dimensional finite element analysis of the temperature field during laser melting of metal powders in additive layer manufacturing. Int J Mach Tool Manu 49:916–923. https://doi.org/10.1016/j.ijmachtools.2009.07.004
13. Ganci M, Zhu W, Buffa G, Fratini L, Bo S, Yan C (2017) A macroscale FEM-based approach for selective laser sintering of thermoplastics. Int J Adv Manuf Technol 91:3169–3180. https://doi.org/10.1007/s00170-017-9998-5
14. Somashekara MA, Naveenkumar M, Kumar A, Viswanath C, Simhambhatla S (2017) Investigations into effect of weld-deposition pattern on residual stress evolution for metallic additive manufacturing. Int J Adv Manuf Technol 90:2009–2025. https://doi.org/10.1007/s00170-016-9510-7
15. Kundakcioglu E, Lazoglu I, Rawal S (2016) Transient thermal modeling of laser-based additive manufacturing for 3D freeform structures. Int J Adv Manuf Technol 85(1):493–501. https://doi.org/10.1007/s00170-015-7932-2
16. Wang Z, Denlinger E, Michaleris P, Stoica AD, Ma D, Beese AM (2017) Residual stress mapping in Inconel 625 fabricated through additive manufacturing: Method for neutron diffraction measurements to validate thermomechanical model predictions. Mater Des 113:169–177. https://doi.org/10.1016/j.matdes.2016.10.003
17. Sih SS, Barlow JW (2004) The prediction of the emissivity and thermal conductivity of powder beds. Part Sci Technol 22(3):291–304. https://doi.org/10.1080/02726350490501682a
18. Mills KC (2002) Recommended Values of Thermophysical Properties for Selected Commercial. Woodhead Publishing, Cambridge